RSC Advances

PAPER

View Article Online
View Journal | View Issue

Cite this: *RSC Adv.*, 2018, **8**, 3243

Flexible ultra-sensitive and resistive NO_2 gas sensor based on nanostructured $Zn_{(x)}Fe_{(1-x)2}O_4$

Solleti Goutham,[a] Kishor Kumar Sadasivuni,[b] Devarai Santhosh Kumar[c] and Kalagadda Venkateswara Rao *[a]

Received 21st September 2017
Accepted 30th December 2017

DOI: 10.1039/c7ra10478b

rsc.li/rsc-advances

Low concentration gas detection, rapid response time and low working temperature are anticipated for a varied range of toxic gas detection applications. Conversely, the existing gas sensors suffer mostly from a high working temperature along with a slow response at low concentrations of analytes. Here, we report an ultrasensitive flexible nanostructured $Zn_{(x)}Fe_{(1-x)2}O_4$ ($x = 0.1$, 0.5 and 0.9) based chemiresistive sensor for nitrogen dioxide (NO_2) detection. We evince that the prepared flexible sensor $Zn_{(0.5)}Fe_{(0.5)2}O_4$ has detection potential as low as 5 ppm at a working temperature of 90 °C in a short phase. Further, the $Zn_{(0.5)}Fe_{(0.5)2}O_4$ sensor exhibits excellent selectivity, stability and repeatability. The optimized sensor sensing characteristics can be helpful in tremendous development of foldable mobile devices for environmental monitoring, protection and control.

1. Introduction

There is a high interest in the discovery of novel nanomaterials in order to develop rapid response and extremely sensitive solid-state gas sensors. Semiconductor metal oxide materials are an alternative to conventional sensing materials due to their exceptional characteristics of easy synthesis, cost-effectiveness and low power consumption. These materials are the best candidates to detect poisonous, toxic, flammable, explosive and harmful gases. The gas sensor working principle involves the surface adsorbed atmospheric oxygen species interaction with analyte gas molecules, leading to redox reactions on the semiconductor, such as ZnO,[1,2] WO_3,[3,4] In_2O_3,[5,6] SnO_2 (ref. 7–10) and Fe_2O_3 (ref. 11,12) (n-type), and NiO[13] and CoO_3O_4 (ref. 14) (p-type) gas sensors. In sensing application crucial roles are performed by properties regarding oxides of semiconductor like pores, grain size, crystalline size, film thickness, layers, and surface to volume ratio.[15,16] Furthermore, if the prepared sensing material is porous, the targeted analyte molecules can easily penetrate the material and react with the total volume of the material by enhancing the sensor response tremendously.[17] Thus, sufficient attention has been concentrated on controlling the structural and morphological parameters of nanomaterials with high-energy surfaces[18,19] and decreased crystalline size,[20] which are gaining special attention, such as oxide composites, core–shell heterostructure nanotubes,[21,22] 3D structures[23,24] and doping.[25]

Spinel ferrites are the basic functional material used in a variety of cutting-edge technological applications because it is exceptionally good catalyst and has simple synthesis. Additionally it is very economical and eco-friendly in nature.[26] $ZnFe_2O_4$ has been widely used with lithium-ion batteries as the anode materials for the past few years. Nanostructured $ZnFe_2O_4$ is a gas sensing material with rapid response and excellent selectivity towards oxidizing and reducing gases. The scientists working on the intrinsic association between shape, structure and gas sensing characteristics have produced essential adaptable synthetic strategies, where these properties of $ZnFe_2O_4$ can be tailored with designed functionalities. In this regard, the preparation of nanostructured $ZnFe_2O_4$ with exclusive microstructures is escalating its possible gas sensor applications.

In the present paper, a simple sol–gel auto combustion method was used to synthesize nanostructured $Zn_{(x)}Fe_{(1-x)2}O_4$ ($x = 0.1$, 0.5 and 0.9).[27] As a result, a large specific surface area pore size was exhibited by the prepared $ZnFe_2O_4$ materials. A flexible device was fabricated by using a simple drop drying technique. Additionally, NO_2 gas sensing characteristics were investigated with various working temperatures. We proved that a nanostructured flexible $Zn_{(x)}Fe_{(1-x)2}O_4$ ($x = 0.5$) based sensor shows a high response at an operating temperature of 90 °C, with excellent selectivity, good stability and reproducibility.

2. Experimental section

2.1 Synthesis of nanostructured $Zn_{(x)}Fe_{(1-x)2}O_4$ ($x = 0.1$, 0.5 and 0.9)

A sol–gel-auto combustion technique was employed to prepare nanostructured $Zn_{(x)}Fe_{(1-x)2}O_4$ ($x = 0.1$, 0.5 and 0.9).[27] In this method, the exothermic reaction of xerogel, which is an aqueous

[a]*Nano Electronics Laboratory, Centre for Nano Science and Technology, JNT University Hyderabad, Kukatpally, Hyderabad-500085, Telangana State, India. E-mail: kalagadda2003@jntuh.ac.in; Tel: +91 9440858664*

[b]*Center for Advanced Materials, Qatar University, P. O. Box 2713, Doha, Qatar*

[c]*Department of Chemical Engineering, IIT – Hyderabad, Kandi-502285, Telangana, India*

solution of metal nitrates (zinc nitrate and iron nitrate) and fuel (glycine) was carried out. All the reagents were of analytical grade from Sigma-Aldrich, USA. An appropriate amount of nitrates and fuel were dissolved in distilled water under constant stirring at 80 °C according to the stoichiometric composition of the fuel to oxidizer ratio. After 25–30 min a brown colored thick gel was formed. The obtained solution was placed on a hot plate at 180 °C to initiate the combustion, then it was ignited to form a lightweight powder and annealed at 650 °C for 5 h.

2.2 Characterization

The structural analysis of the nanostructured $Zn_{(x)}Fe_{(1-x)2}O_4$ (x = 0.1, 0.5 and 0.9) powder was made with a Bruker-D8 X-ray diffractometer (XRD) using Cu Kα_1 radiation. The optical property of absorbance was calculated by a UV-visible double beam spectrophotometer (Systronic-2203). Fourier transform infrared spectroscopy (FT-IR) (PerkinElmer L160000A) in the wavelength range of 500–4000 cm^{-1} was also used for the structural elucidation. The morphology and elemental composition were observed by a Carl Zeiss (Merlin compact 60-27) field emission scanning electron microscope (EDX and FESEM). Particle size and morphology were further confirmed by transmission electron microscopy (TEM) (Philips, Holland TEM instrument) operated at an accelerating voltage of 120 kV. Resistance and voltage were measured using the Keithley multimeter (2750).

2.3 Device fabrication and construction of in-house sensor testing unit

The samples were coated with a drop drying method on flexible electrodes prior to testing, which can be described as follows. Initially, an approximate amount of the as-prepared $Zn_{(x)}Fe_{(1-x)2}O_4$ (x = 0.1, 0.5 and 0.9) nanostructured powder was mixed with dimethylformamide to prepare the homogeneous paste and coated onto flexible pre-patterned interdigitated electrodes (IDEs). This was then allowed to dry at room temperature, and the device was calcinated at 150 °C for 3 h to enhance its stability. Finally, the fabricated device was connected to a Keithley multimeter (2750) in an in-house dynamic gas sensing setup. The sensing examination of the developed gas sensor was examined by a sensor testing unit, which was explained comprehensively in our earlier paper.[28] The construction of the in-house sensing setup is schematically demonstrated in Fig. 1. The sensor response was calculated as $S = (R_a - R_g)/R_a$ for oxidizing gases or $(R_g - R_a)/R_g$ for reducing gases, where R_a is the resistance value in absence of air and R_g is the resistance in the presence of the analyte gas. The sensor was analyzed in both flat and bending position to demonstrate the flexibility of the sensor. A bending angle of 60° was used to determine the flexibility.

3. Results and discussion

3.1 Structural and morphological characteristics

The X-ray diffraction (XRD) spectra of the pre-synthesized nanostructured $Zn_{(x)}Fe_{(1-x)2}O_4$ (x = 0.1, 0.5 and 0.9) is shown in Fig. 2a. The $Zn_{(x)}Fe_{(1-x)2}O_4$ (x = 0.5) deflection peaks were in good

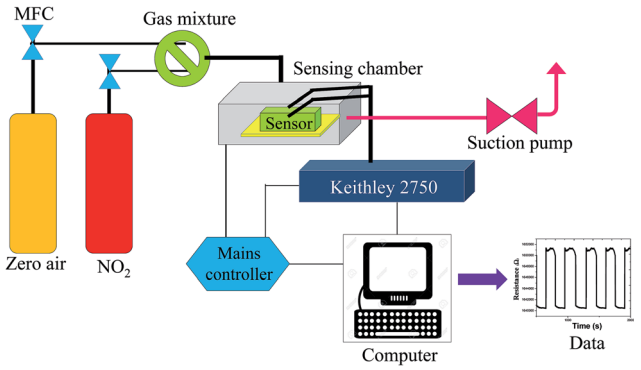

Fig. 1 Schematic of in-house setup for gas sensing.

agreement with the standard JCPDS no. 89-1012, which shows the product is highly pure and has no other impurities. This indicates that metal nitrates were fully transformed into $ZnFe_2O_4$ at 650 °C. Whereas in the case of the $Zn_{(x)}Fe_{(1-x)2}O_4$ (x = 0.1 and 0.9) materials, due to their compositional variations, a slight peak shift was noticed (Fig. 2a). Nanostructured $Zn_{(x)}Fe_{(1-x)2}O_4$ (x = 0.5) deflection peaks were comparatively broadened, indicating its small crystallite size. The average crystal sizes of nanostructured $Zn_{(x)}Fe_{(1-x)2}O_4$ (x = 0.1, 0.5 and 0.9) are about 21.5 nm, 16.8 nm and 18.7 nm, respectively. The crystalline size was estimated by the Debye–Scherrer formula $D = 0.89\lambda/\beta \cos\theta$ (where λ = 1.54060 Å, θ is the Bragg angle and β is the peak full width at half maximum).

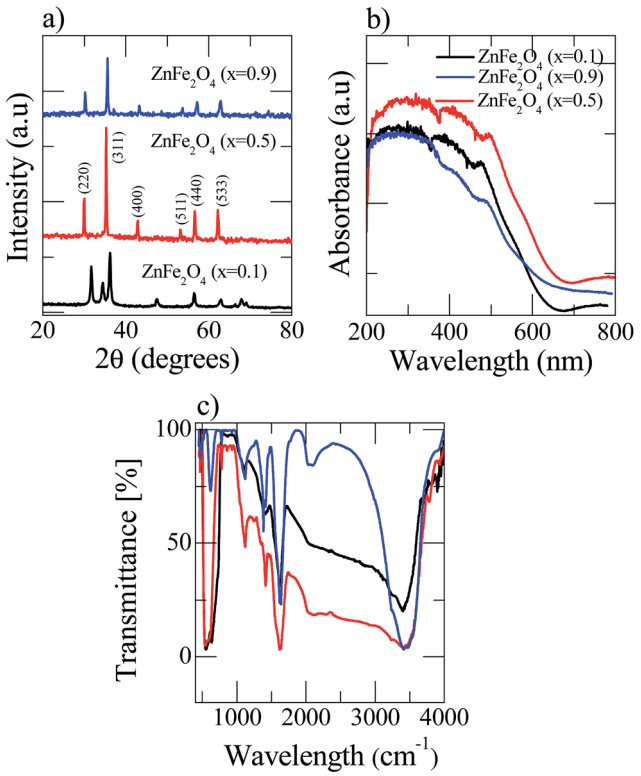

Fig. 2 Room temperature analysis of the three as-prepared $Zn_{(x)}Fe_{(1-x)2}O_4$ (x = 0.1, 0.5 and 0.9) samples (a) XRD patterns (b) UV-visible spectroscopy and (c) Fourier transform infrared spectroscopy.

The UV-vis spectra of the $Zn_{(x)}Fe_{(1-x)2}O_4$ ($x = 0.1$, 0.5 and 0.9) are shown in Fig. 2b and a strong absorption was observed for all the prepared samples. $Zn_{(x)}Fe_{(1-x)2}O_4$ ($x = 0.5$) exhibits peak shift from UV to visible light region and reveals the nanostructured $Zn_{(x)}Fe_{(1-x)2}O_4$ ($x = 0.5$) having a higher efficiency to absorb visible light than $Zn_{(x)}Fe_{(1-x)2}O_4$ ($x = 0.1$ and 0.9). Moreover, the absorption spectrum of the $Zn_{(x)}Fe_{(1-x)2}O_4$ ($x = 0.5$) material contained both regions (UV and visible) of $Zn_{(x)}Fe_{(1-x)2}O_4$ ($x = 0.1$ and 0.9). These results show that an equal composition of precursor material causes expansion and enhancement of the photoresponse to the visible region. Hence, we observe that the photocatalytic activity of the prepared $Zn_{(x)}Fe_{(1-x)2}O_4$ ($x = 0.5$) was superior to that of $Zn_{(x)}Fe_{(1-x)2}O_4$ ($x = 0.1$ and 0.9) in visible light.

A Fourier transform infrared (FTIR) spectrophotometer was used to analyze the $Zn_{(x)}Fe_{(1-x)2}O_4$ ($x = 0.1$, 0.5 and 0.9) nanostructured materials in the range from 500 to 4000 cm^{-1} and the results are shown in Fig. 2c. The FTIR spectra of all three samples show the peak at 1274 cm^{-1} represented =C–H in-plane stretching. The peak at 923 cm^{-1} is from C–C out-of-plane stretching vibrations[29] and the broad band observed at 3430 cm^{-1} is related to O–H vibrations. Peaks at vibrations around 500 cm^{-1} are attributed to Fe–O and Zn–O vibrations.[30]

The nanostructured $Zn_{(x)}Fe_{(1-x)2}O_4$ ($x = 0.1$, 0.5 and 0.9) morphologies are shown in Fig. 3a–c and the structures were analyzed by field emission scanning electron microscopy (FESEM). All the samples exhibited nanocrystalline and mixed shaped cellular structures. A qualitative examination reveals that $Zn_{(x)}Fe_{(1-x)2}O_4$ ($x = 0.5$) material is smaller, with minute interstices of a more distinctive and uniform nature than those of the $Zn_{(x)}Fe_{(1-x)2}O_4$ ($x = 0.1$ and 0.9) materials. An equal amount of precursor, *i.e.*, $Zn_{(0.5)}Fe_{(0.5)2}O_4$ (Fig. 3b) displayed

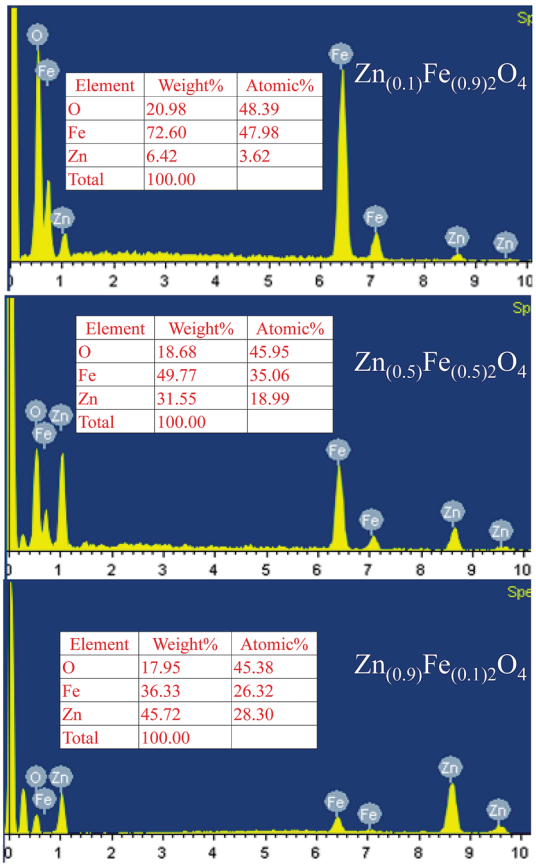

Fig. 4 EDS spectrum and composition data of the $Zn_{(x)}Fe_{(1-x)2}O_4$ ($x = 0.1$, 0.5 and 0.9) samples.

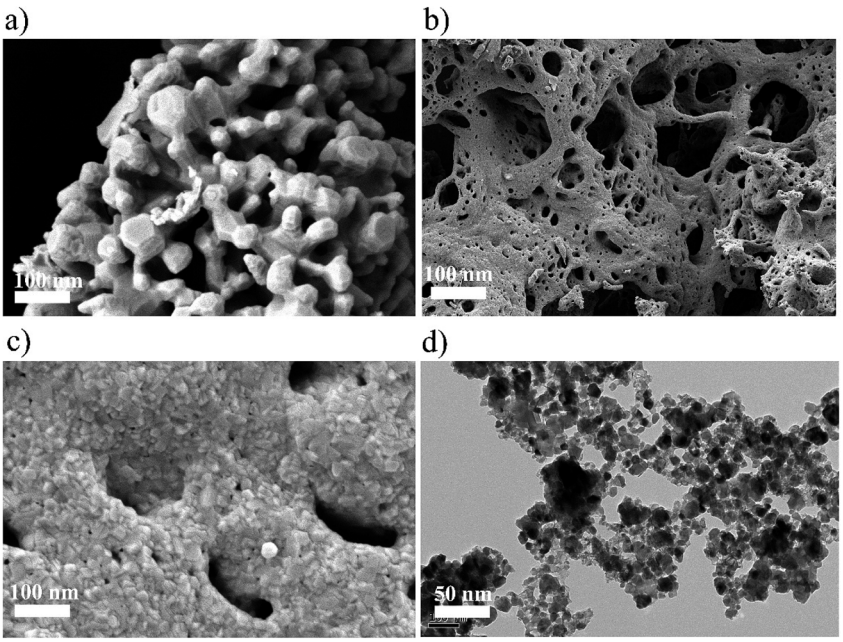

Fig. 3 (a) FESEM image of $Zn_{(0.1)}Fe_{(0.9)2}O_4$ (b) FESEM image of $Zn_{(0.5)}Fe_{(0.5)2}O_4$ (c) FESEM image of $Zn_{(0.9)}Fe_{(0.1)2}O_4$ and (d) typical HRTEM image of $Zn_{(0.5)}Fe_{(0.5)2}O_4$.

a necked type particle cluster and porous nature. The crystalline sizes of the samples analyzed by FE-SEM exhibit an average of 29.3 nm, 20.4 nm and 22.5 nm for nanostructured $Zn_{(x)}Fe_{(1-x)}{}_2O_4$ (x = 0.1, 0.5 and 0.9), respectively. These values were compared with XRD measurements and where observed to be in good agreement. The typical HRTEM of the nanostructured $Zn_{(x)}Fe_{(1-x)2}O_4$ (x = 0.5) is illustrated in Fig. 3d. The size and structure of the material were in harmony with the FESEM results. These results confirm a massive amount of particles are of a nano size and assembled to form a spherical structure. Fig. 4 represents the elemental analysis of the nanostructured $Zn_{(x)}Fe_{(1-x)2}O_4$ (x = 0.1, 0.5 and 0.9) materials and evidences the presence of Zn, Fe and O.

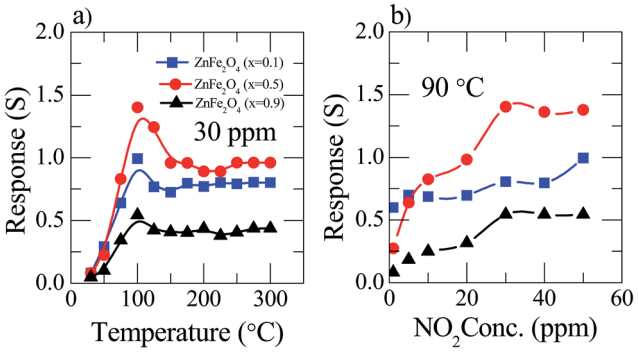

Fig. 5 Sensor response of $Zn_{(x)}Fe_{(1-x)2}O_4$ (x = 0.1, 0.5 and 0.9) of (a) to 30 ppm NO_2 gas at different operating temperatures (b) constant 90 °C temperature at various NO_2 gas concentration.

3.2 Gas sensing properties

The present study deals with the advantages of the pre-synthesized nanostructured materials $Zn_{(x)}Fe_{(1-x)2}O_4$ (x = 0.1, 0.5 and 0.9) as NO_2 sensing substances and their characteristics. In a chemiresistive gas sensor, the sensitivity mainly depends upon the operating temperature. Thus, the responses of $Zn_{(x)}Fe_{(1-x)2}O_4$ (x = 0.1, 0.5 and 0.9) based sensors were measured by changing the temperature from room temperature to 300 °C at a constant gas concentration of 30 ppm and the related examined results are illustrated in Fig. 5a. In the figure, it is clearly shown that cone shape curves represent that the

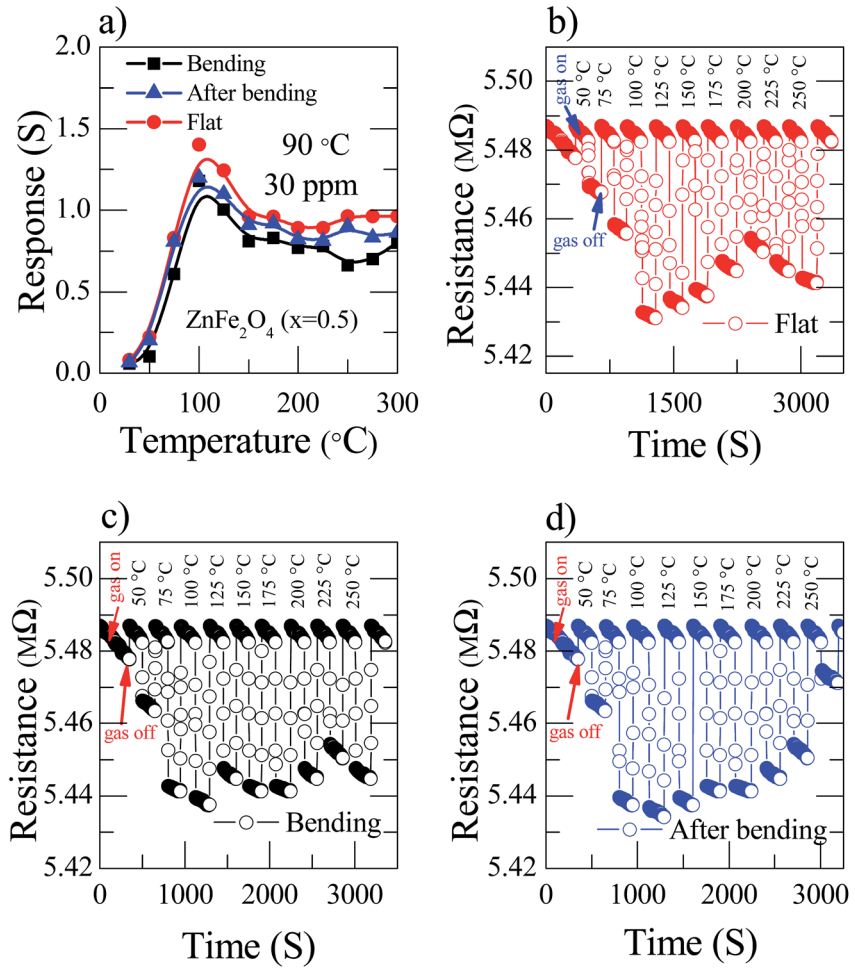

Fig. 6 (a) $Zn_{(0.5)}Fe_{(0.5)2}O_4$ sensor response at 30 ppm NO_2 gas at 90 °C temperature and different bending conditions (red color stands for flat, black for bending and blue for after bending) (b–d) dynamic response of the recovery behavior of the $Zn_{(0.5)}Fe_{(0.5)2}O_4$ sensors towards 30 ppm NO_2 gas at 90 °C flat, bending and after bending conditions, respectively.

initial NO_2 response was enhanced with operating temperature and reaches its highest value for about 90 °C, and afterwards reduces slowly. The threshold temperature for the sensor was observed at 90 °C. Among all three prepared samples, $Zn_{(x)}Fe_{(1-x)2}O_4$ (x = 0.1, 0.5 and 0.9), the maximum response was observed for the equal amount of precursor material *i.e.*, $Zn_{(x)}Fe_{(1-x)2}O_4$ (x = 0.5). The obtained increase–decrease result responses can be described as follows: at room temperature, NO_2 gas molecules partially interact with the surface absorbed atmospheric oxygen molecules, which gives a lower response. Whereas, with increasing the operating temperature the rate of reaction becomes higher and there is an increase in the oxygen ions on the sensor surface from the absorbed atmospheric oxygen species ($O_{2(gas)} \rightarrow O_{2(ads)} \rightarrow O_{2(ads)}^{-} \rightarrow 2O_{(ads)}^{-}$) responsible for the maximum response. From the result, 90 °C is the optimum working temperature for the selected nanostructured $Zn_{(x)}Fe_{(1-x)2}O_4$ (x = 0.5). In the case of $Zn_{(x)}Fe_{(1-x)2}O_4$ (x = 0.1 and 0.9), the sensor response observed was 0.74 and 0.54%, respectively, for 90 °C at 30 ppm and comparatively these sensitivity results were a much smaller response than the sensor response (1.41%) of the equal ratio precursor ($Zn_{(0.5)}Fe_{(0.5)2}O_4$). The reason behind this kind of behavior might be due to the $Zn_{(0.5)}Fe_{(0.5)2}O_4$ sensor having enough porosity so that NO_2 gas can easily penetrate inside the sensing material throughout the surface. The nanostructured $Zn_{(x)}Fe_{(1-x)2}O_4$ (x = 0.1 and 0.9) sensor material has a low porosity compared to the $Zn_{(0.5)}Fe_{(0.5)2}O_4$ materials.

The response of the $Zn_{(x)}Fe_{(1-x)2}O_4$ (x = 0.1, 0.5 and 0.9) sensor variations along with the NO_2 gas dilutions was examined at an optimum working temperature (Fig. 5b). It is observed that as the gas concentration value increases slowly from 1 ppm, the sensor response increased up to 30 ppm and then saturated. This kind of sensing behavior can be estimated as follows: a very low surface interaction at a minute gas concentration leads to a low sensor response. The sensitivity increased stepwise when the gas concentration increased to create an enhanced sensor surface interaction, leading to a rising response at a critical concentration, *i.e.* 30 ppm. Followed by a increased NO_2 gas concentration, the sensor surface was fully covered by and therefore had no possibility to react with new molecules due to the saturation level.

The tremendous fabricated current device is solely transparent and mechanically flexible. To investigate the nanostructured $Zn_{(0.5)}Fe_{(0.5)2}O_4$ sensor, flexibility properties were measured in flat (red), bending (black) and after bending (blue) conditions with a bending radius of 60° for 30 ppm NO_2 at 90 °C. Fig. 6a illustrates the sensor response based on flexibility and temperature variations. The response of the sensor device decreased moderately while bending due to the reduction of the sensitive surface area. Fascinatingly, the fabricated device did not deteriorate considerably after these mechanical transformations. Moreover, the few dynamic cycles of the response–recovery of the flexible sensor shown in Fig. 6b–d depicted different conditions at various temperatures for 30 ppm NO_2.

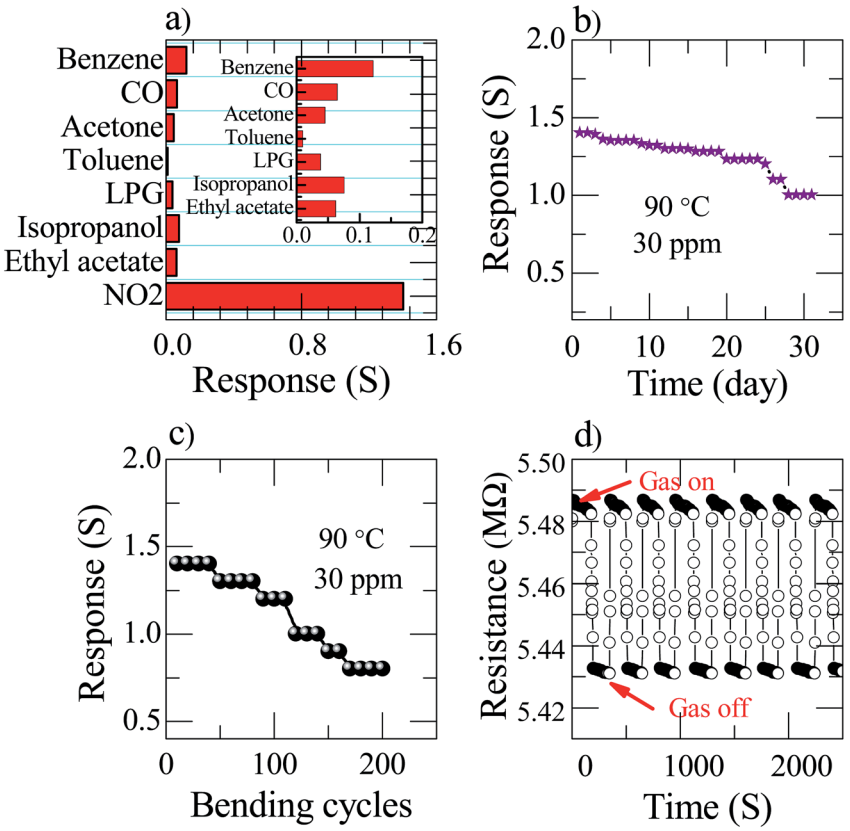

Fig. 7 $Zn_{(0.5)}Fe_{(0.5)2}O_4$ sensor at an operating temperature of 90 °C for 30 ppm (a) selectivity. The inset represents the response to various analytes (small scale) (b) stability (c) bending test (d) reproducibility.

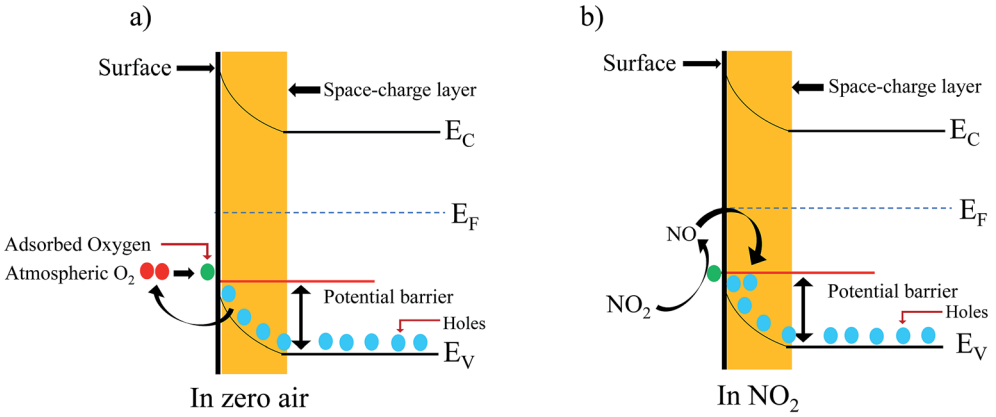

Fig. 8 (a and b) Schematic illustration of the air and NO_2 mechanisms for nanostructured $ZnFe_2O_4$.

Table 1 The present study compared with the literature on $ZnFe_2O_4$ based NO_2 gas sensor

S. No.	Material	Substrate	Operating temperature (°C)	Gas concentration	Reference
1	WO_3	Hard	27	320 ppb	34
2	Graphene	Hard	27	25 ppm	35
3	ZnO	Hard	27	16 ppm	36
4	S/graphene	Hard	27	100 ppm	37
5	$CoTa_2O_6$	Hard	650	100 ppm	38
6	Ce/NiO	Hard	150	40 ppm	39
7	(rGO)–In_2O_3	Flexible	150	500 ppb	40
8	$Zn_{(0.5)}Fe_{(0.5)2}O_4$	Flexible	90	5 ppm	Present work

The nanostructured $Zn_{(0.5)}Fe_{(0.5)2}O_4$ sensor selectivity was studied by exposing different analytes, such as benzene, carbon monoxide, acetone, toluene, LPG, isopropanol and ethyl acetate, as shown in Fig. 7a. The concentration of all the analytes was maintained constant, *i.e.* 30 ppm at 90 °C. The sensor response against NO_2 was remarkably higher than against other analytes. This analysis provides the information regarding the high selectivity of the sensor towards NO_2. This is due to the chemisorbed atmospheric oxygen present on the sensor surface effectively initiating a high response towards NO_2. In the practical application of gas sensors, long-term stability is one of the essential characteristic parameters. Therefore, the response of the prepared flexible $Zn_{(0.5)}Fe_{(0.5)2}O_4$ sensor to 30 ppm of NO_2 at a temperature of 90 °C was examined for 30 days as illustrated in Fig. 7b. In that period of time, the sensor response was recorded with only a little fluctuation. Therefore, fabrication of attractive and promising sensor with an excellent durability is possible with this technique. These sensors are very useful in a direct industrial application. Bending tests were implemented on the sensor during the test to understand the flexibility of the sensor. After two hundred repeats of bending of the prepared flexible sensor, the device did not have a large deviation of response (Fig. 7c). To examine the repeatability of the flexible sensor, the $Zn_{(0.5)}Fe_{(0.5)2}O_4$ device were exposed to seven cycles of 30 ppm NO_2 and the dynamic resistance responses are shown in Fig. 7d. The test revealed that the sensor response is constantly maintained after several exposure cycles. From the obtained results, the sensor shows good reproducibility for a long time, which confirms the stability of the prepared gas sensor towards NO_2.

3.3 Gas sensing mechanism

A well-known p-type semiconductor oxide[31] such as $ZnFe_2O_4$, works as a sensor and the functioning mechanism involved is based on the change in resistance of the atmospheric oxygen molecule chemisorption on the surface of the sensing material.[32,33] $ZnFe_2O_4$ contains holes as the major charge carrier. Initially, when the flexible $ZnFe_2O_4$ sensor is exposed to zero air, the atmospheric oxygen molecules in the form of $O_{2(ads)}^-$, $O_{(ads)}^-$ and $O^{2-}{}_{(ads)}$ adsorb on the surface of the sensor. The sensor resistance increases due to the formation of a thick electron space charge layer on the surface (Fig. 8a). Followed by the exposure to an oxidizing gas, *i.e.* NO_2 (electron accepting), molecules interact with adsorbed oxygen molecules, which leads to a decrease in resistance (Fig. 8b). The flexible $ZnFe_2O_4$ gas sensor performance towards NO_2 gas is compared with previously reported $ZnFe_2O_4$ gas sensor for various analytes as listed in Table 1.

4. Conclusion

In summary, a sol–gel auto combustion method was used for the preparation of nanostructured flexible $Zn_{(x)}Fe_{(1-x)2}O_4$ (x = 0.1, 0.5 and 0.9), which were coated on a pre-patterned flexible electrode by a simple drop drying process and heated

afterwards. The synthesized material was examined as a sensing material for the possible chemiresistive gas sensing application. It was found that the equal concentration of precursor material ($Zn_{(x)}Fe_{(1-x)2}O_4$ ($x = 0.5$)) used in device exhibited an ultra-high sensing performance and excellent long-term stability, selectivity and reproducibility towards 5 ppm of NO_2 at a working temperature of 90 °C.

Conflicts of interest

There are no conflicts to declare.

Acknowledgements

The author (KVR) is thankful to the Science and Engineering Research Board (SERB) – Department of Science and Technology (DST), Government of India, [Project No. SB/EMEQ-183/2013] for the generous financial support.

References

1 N. Tamaekong, C. Liewhiran, A. Wisitoraat and S. Phanichphant, *Sensors*, 2010, **10**, 7863.
2 X. W. Li, X. Zhou, H. Guo, C. Wang, J. Y. Liu, P. Sun, F. M. Liu and G. Y. Lu, *ACS Appl. Mater. Interfaces*, 2014, **6**, 18661.
3 X. L. Li, T. J. Lou, X. M. Sun and Y. D. Li, *Inorg. Chem.*, 2004, **43**, 5442.
4 L. Wang, A. Teleki, S. E. Pratsinis and P. I. Gouma, *Chem. Mater.*, 2008, **20**, 4794.
5 X. H. Sun, H. R. Hao, H. M. Ji, X. L. Li, S. Cai and C. M. Zheng, *ACS Appl. Mater. Interfaces*, 2014, **6**, 401.
6 K. Inyawilert, A. Wisitsora-at, A. Tuantranont, P. Singjai, S. Phanichphant and C. Liewhiran, *Sens. Actuators, B*, 2014, **192**, 745.
7 L. Renard, J. Brotz, H. Fuess, A. Gurlo and R. Riedel, *ACS Appl. Mater. Interfaces*, 2014, **6**, 17093.
8 L. Rwnard, O. Babot, H. Saadaoui, H. Fuess, J. Brota, A. Gurlo, E. Arveux, A. Klein and T. Toupance, *Nanoscale*, 2012, **4**, 6806.
9 S. Singkammo, A. Wisitsoraat, C. Sriprachuabwong, A. Tuantranont, S. Phanichphant and C. Liewhiran, *ACS Appl. Mater. Interfaces*, 2015, **7**, 3077.
10 M. Punginsang, A. Wisitsora-at, A. Tuantranont, S. Phanichphant and C. Liewhiran, *Sens. Actuators, B*, 2015, **210**, 589.
11 S. Agarwala, Z. H. Lim, E. Nicholson and G. W. Ho, *Nanoscale*, 2012, **4**, 194.
12 Z. Y. Sun, H. Q. Yuan, Z. M. Liu, B. X. Han and X. R. Zhang, *Adv. Mater.*, 2005, **17**, 2993.
13 H. J. Kim, K. I. Choi, K. M. Kim, C. W. Na and J. H. Lee, *Sens. Actuators, B*, 2012, **171**, 1029.
14 Z. F. Dou, C. Y. Cao, Y. Chen and W. G. Song, *Chem. Commun.*, 2014, **50**, 14889.
15 N. Wang, H. Xu, L. Chen, X. Gu, J. Yang and Y. J. Qian, *J. Power Sources*, 2014, **247**, 163.
16 K. K. Sadasivuni, D. Ponnamma, H. U. Ko, H. C. Kim, L. Zhai and J. Kim, *Sens. Actuators, B*, 2016, **233**, 633.
17 J. G. Thangamani, K. Deshmukh, K. K. Sadasivuni, K. Chidambaram, M. B. Ahamed, D. Ponnamma, M. A. A. AlMaadeed and S. K. Khadheer Pasha, *Adv. Mater. Lett.*, 2017, **8**, 196.
18 X. Han, M. Jin, S. Xie, Q. Kuang, Z. Jiang , Y. Q. Jiang, Z. X. Xie and L. S. Zheng, *Angew. Chem.*, 2009, **121**, 9344.
19 J. Liu, X. Chen, W. Wang, Y. Liu, Q. S. Huang and Z. P. Guo, *CrystEngComm*, 2011, **13**, 3425.
20 N. Yamazoe and K. Shimanoe, *J. Electrochem. Soc.*, 2008, **155**, 85.
21 Q. Yu, J. Zhu, Z. Xu and X. T. Huang, *Sens. Actuators, B*, 2015, **213**, 27.
22 D. Ponnamma, K. K. Sadasivuni, M. Strankowski, Q. Guo and S. Thomas, *Soft Matter*, 2013, **43**, 10343.
23 J. G. Thangamani, K. Deshmukh, K. K. Sadasivuni, D. Ponnamma, S. Goutham, K. V. Rao, K. Chidambaram, M. B. Ahamed, A. N. Grace, M. Faisal and S. K. K. Pasha, *Microchim. Acta*, 2017, **184**, 3977.
24 A. Kafy, K. K. Sadasivuni, A. Akther, S. K. Min and J. Kim, *Mater. Lett.*, 2015, **159**, 20.
25 P. Li, Y. Cai and H. Fan, *RSC Adv.*, 2013, **3**, 22239.
26 L. Li, J. Tan, M. Dun and X. Huang, *Sens. Actuators, B*, 2017, **248**, 85–91.
27 A. Sutka and G. Mezinskis, *Front. Mater. Sci.*, 2012, **6**, 128.
28 S. Goutham, D. S. Kumar, K. K. Sadasivuni, J. J. Cabibihan and K. V. Rao, *J. Electron. Mater.*, 2017, **46**, 2334.
29 Z. Shahnavaz, F. Lorestani, Y. Alias and P. M. Woi, *Appl. Surf. Sci.*, 2014, **317**, 622.
30 V. A. M. Brabers, *Phys. Status Solidi B*, 1969, **33**, 563.
31 F. Liu, X. Li, Q. Zhao, Y. Hou, X. Quan and G. Chen, *Acta Mater.*, 2009, **57**, 2684.
32 F. Liu, X. F. Chu, Y. P. Dong, W. B. Zhang, W. Q. Sun and L. M. Shen, *Sens. Actuators, B*, 2013, **188**, 469.
33 G. Y. Zhang, C. S. Li, F. Y. Cheng and J. Chen, *Sens. Actuators, B*, 2007, **120**, 403.
34 C. Zhang, A. Boudiba, C. Bittencourt, R. Snydersb, M. G. Oliviera and M. Debliquy, *Procedia Eng.*, 2012, **47**, 116.
35 Y. Seekaew, D. Phokharatkul, A. Wisitsoraat and C. Wongchoosuk, *Appl. Surf. Sci.*, 2017, **404**, 357.
36 L. Rana, R. Gupta, M. Tomar and V. Gupta, *Sens. Actuators, B*, 2017, **252**, 840.
37 L. Guo and T. Li, *Sens. Actuators, B*, 2018, **255**, 2258.
38 F. Liu, B. Wang, X. Yang, Y. Guan, Q. Wang, X. Liang, P. Sun, Y. Wang and G. Lu, *Sens. Actuators, B*, 2017, **240**, 148.
39 S. R. Gawali, V. L. Patil, V. G. Deonikar, S. S. Patil, D. R. Patil, P. S. Patil and J. Pant, *J. Phys. Chem. Solids*, 2017, **114**, 28.
40 C. W. Na, J. Kim, H. Kim, H. Woo, A. Gupta, H. Kim and J. Lee, *Sens. Actuators, B*, 2018, **255**, 1671.